

Geophysical Research Letters[®]

RESEARCH LETTER

10.1029/2022GL098443

Key Points:

- We used change in concentration along streaklines extracted from remote-sensed imagery to infer instantaneous rates of deposition/erosion
- Our method accurately inverts for deposition rates when applied to synthetic data from a 2D advection-settling model
- We obtained coherent patterns of deposition and erosion based on remote-sensed imagery of Wax Lake Delta, Louisiana

Supporting Information:

Supporting Information may be found in the online version of this article.

Correspondence to:

G. Salter,
gsalter@caltech.edu

Citation:

Salter, G., Passalacqua, P., Wright, K., Feil, S., Jensen, D., Simard, M., & Lamb, M. P. (2022). Spatial patterns of deltaic deposition/erosion revealed by streaklines extracted from remotely-sensed suspended sediment concentration. *Geophysical Research Letters*, 49, e2022GL098443. <https://doi.org/10.1029/2022GL098443>

Received 24 FEB 2022
Accepted 18 MAY 2022

Spatial Patterns of Deltaic Deposition/Erosion Revealed by Streaklines Extracted From Remotely-Sensed Suspended Sediment Concentration

Gerard Salter¹ , Paola Passalacqua² , Kyle Wright² , Sarah Feil³ , Daniel Jensen⁴ , Marc Simard⁴ , and Michael P. Lamb¹ 

¹Division of Geological and Planetary Sciences, California Institute of Technology, Pasadena, CA, USA, ²Department of Civil, Architectural, and Environmental Engineering, University of Texas at Austin, Austin, TX, USA, ³Department of Sedimentology and Environmental Geology, Georg-August-Universität Göttingen, Göttingen, Germany, ⁴Jet Propulsion Laboratory, California Institute of Technology, Pasadena, CA, USA

Abstract Deltas are vulnerable landscapes, making it crucial to understand their spatial patterns of deposition/erosion. Here, we used patterns in suspended sediment concentration (SSC) measured by a NASA airborne spectrometer, AVIRIS-NG, to infer deposition/erosion within Wax Lake Delta, Louisiana. Conceptually, change in SSC within a fluid parcel traveling downstream reflects settling and/or entrainment from the bed. We found that remotely-sensed SSC displays curvilinear features, which we interpret as streaklines. We developed a semi-automated technique for extracting streaklines using a cost function based on SSC and its geometric curvature. We measured SSC change along streaklines, which when combined with flow velocities obtained from a hydrodynamic model, allowed us to infer instantaneous deposition/erosion rates. These rates are realistic in magnitude and record coherent spatial patterns across the delta. Our novel method provides a promising avenue for relating spatial patterns of land change to flow conditions over wide areas in vulnerable deltas.

Plain Language Summary River deltas are naturally low-lying, making them vulnerable to flooding due to sea-level rise. Predicting which regions of a river delta will be most vulnerable in the future requires understanding of how their elevation will change due to deposition and erosion of sediment. Deposition and erosion are difficult to measure, and depend on factors such as sediment supply and flow conditions. Here, we developed a technique to use suspended sediment concentration measured from airborne imagery to infer deposition/erosion. We find coherent spatial patterns, which we relate to flow conditions and sediment supply. Our novel method provides a promising avenue for relating spatial patterns of land change to flow conditions over wide areas in vulnerable river deltas. Future airborne and satellite-based measurements will provide new opportunities to apply these methods to other river deltas globally.

1. Introduction

River deltas are dynamic landscapes. Their bathymetric evolution reflects spatial patterns of deposition and erosion (Shaw et al., 2013). Most existing methods to measure sediment transport are localized, making it difficult to assess spatial patterns. One way to measure spatial patterns of deposition and erosion is through differencing between elevation maps. For example, this approach has been applied in Wax Lake Delta, Louisiana, an active sub-delta of the Mississippi River Delta, Louisiana, USA. These studies reveal patterns such as channel and delta front deposition and erosion (Shaw & Mohrig, 2014), island levee deposition (Wagner et al., 2017), and delta-wide sediment export (Whaling & Shaw, 2020). However, these methods rely on elevation maps acquired months to years apart, making it impossible to mechanistically link specific hydrodynamic or environmental conditions to bathymetric change. Bathymetric change is sensitive to a variety of factors, including floods, cold fronts, hurricanes, tides, wind, and vegetation (Bevington et al., 2017; Carle et al., 2015; Styles et al., 2021). Remote-sensed synoptic measurement of deposition and erosion would provide a way to directly link specific processes to resulting patterns of bathymetric evolution.

Several studies have derived relationships between suspended sediment concentration (SSC) and remotely-sensed spectral radiance in order to generate maps of SSC (Curran & Novo, 1988; Peckham, 2008; Van der Wal et al., 2010). Unfortunately, coarse spatial resolution limits their applicability to finer-scale spatial patterns.

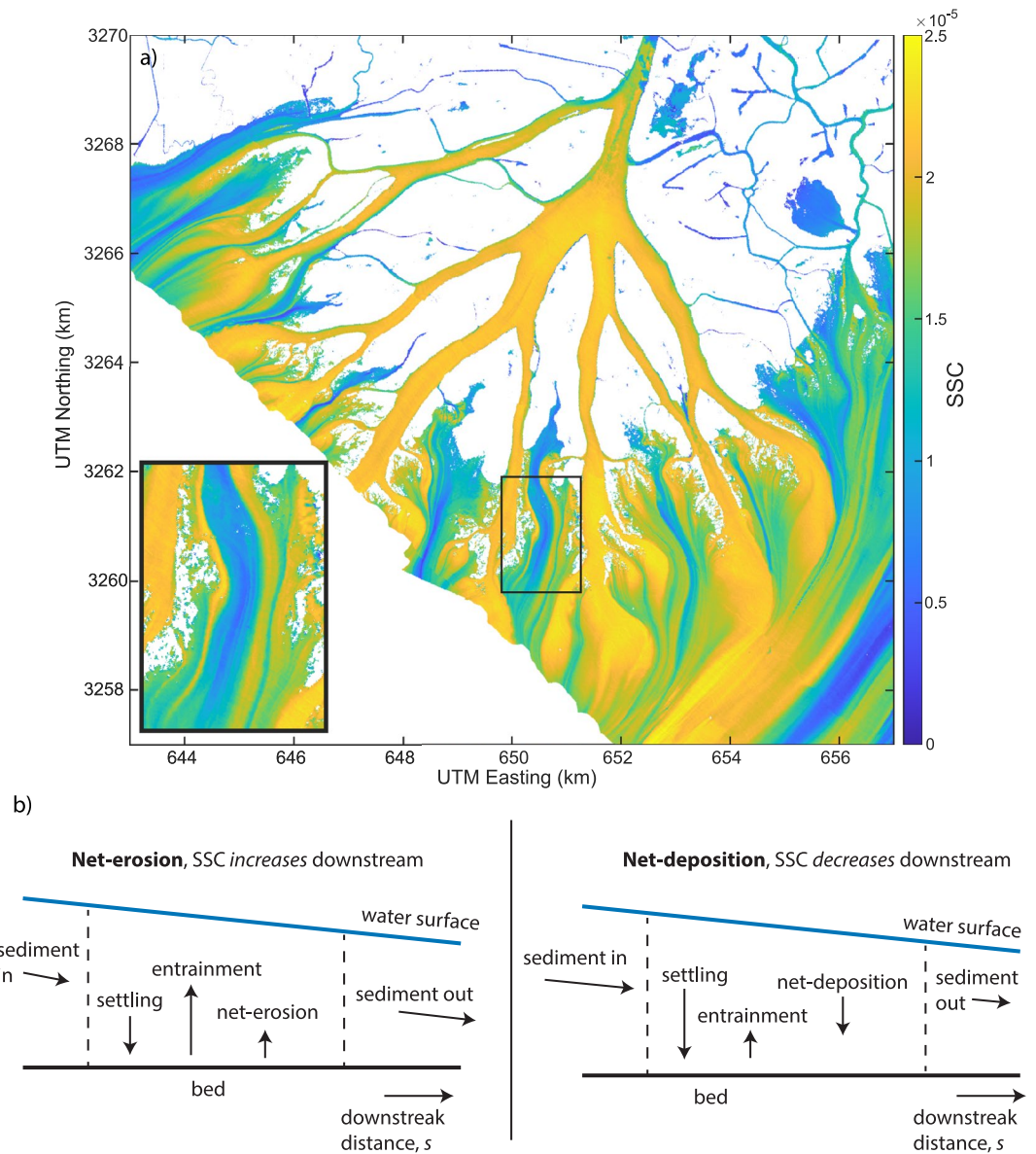


Figure 1. (a) Map of remote-sensed suspended sediment concentration (SSC) over Wax Lake Delta, Louisiana. Data from Jensen et al. (2019), based on AVIRIS-NG flyover from 18 October 2016 between 15:25 and 15:41 GMT. (b) Schematic illustrating how change in SSC along a streakline can be used to infer net-deposition or net-erosion. The difference between the settling and entrainment fluxes gives the net-deposition rate. SSC increase from upstream to downstream implies net-erosion, and SSC decrease implies net-deposition.

However, several recent studies have used airborne spectrometry to generate high-resolution maps of SSC and/or turbidity (Fichot et al., 2016; Olmanson et al., 2013). In particular, Jensen et al. (2019) used an empirical hyperspectral approach with a 5 m resolution to generate maps of SSC in a region of the Mississippi River Delta surrounding the Atchafalaya River and Wax Lake Delta, Louisiana.

In this paper we develop a novel method for inferring deposition and erosion from remote-sensed SSC. We take advantage of curvilinear patterns of high and low sediment concentration, as seen in Figure 1a, which we interpret as streaklines, that is, curves that are formed by a series of fluid parcels originating at a point. Recent studies have used biogenic streaklines in Wax Lake Delta to infer flow direction (Cathcart et al., 2020; Shaw et al., 2016). In contrast to these studies, the streaklines revealed in Figure 1a are features in the synoptic SSC field itself, arising from the contrast between low-concentration waters draining island interiors and high-concentration waters in the

delta primary channels. Although SSC data of sufficient spatial and spectral resolution to reveal these patterns are currently rare, ongoing and future missions such as the NASA Delta-X mission (Simard et al., 2020) and the Surface Biology and Geology (Cawse-Nicholson et al., 2021) will provide new opportunities to apply our methods. Our methods could be used in other coastal, wetland, or deltaic system with visible streaklines present in remote-sensed SSC imagery, providing a novel way to link specific conditions to spatial patterns of deposition/erosion.

2. Methods

We developed a method for extracting streaklines from remote-sensed SSC, and used the change in SSC along streaklines to reveal patterns of deposition and erosion in Wax Lake Delta, Louisiana. As illustrated in Figure 1b, according to mass balance, the change in SSC of a depth-averaged fluid parcel as it travels downstream reflects exchange between the flow and the bed. Therefore, increasing SSC along a streakline implies that sediment is entering the flow from the bed, that is, erosion, whereas decreasing SSC implies deposition.

We used SSC empirically derived by Jensen et al. (2019) using hyperspectral data from a NASA airborne spectrometer, AVIRIS-NG. In particular, we used the 18 October 2016 AVIRIS-NG flyover of Wax Lake Delta, Louisiana, which occurred between 15:25 and 15:41 GMT. Empirical models based on in situ water samples paired with spectroscopic measurements are widely implemented due to their simplicity and explanatory power, but generally cannot be applied beyond a specific location/time due to variation in the optical properties of water bodies. This study was unique in that it took advantage of high spectral-resolution data to develop a partial least squares model for SSC based on spectral derivatives that diminishes the impact of optically-active constituents on SSC retrievals, enabling greater transferability. Additionally, they used the spectroradiometric calibration process described in Chapman et al. (2019) and atmospheric correction described in Thompson et al. (2015).

2.1. Streakline Extraction

We developed a semi-automated method for extracting streaklines from a map of remote-sensed SSC, c , using a cost function approach inspired by Passalacqua et al. (2010). First, we applied a Perona-Malik filter to the image of c to remove noise while preserving the sharp-gradient features of the original image (Passalacqua et al., 2010; Perona & Malik, 1990). Next, we computed the geometric curvature of c , $\kappa = \nabla \cdot (\nabla c / \|\nabla c\|)$, which can be interpreted as the curvature of the contour lines of c . The geometric curvature highlights the centerlines of streaks. Positive geometric curvature corresponds to “valleys” of SSC, that is, low concentration streaks, and negative geometric curvature corresponds to “ridges,” that is, high concentration streaks (Figure 2a). Similarly to Passalacqua et al. (2010), we defined a cost function and extracted streaklines as curves of minimum cost, that is, geodesic curves (Figure 2b). The method was semi-automated in that we manually selected start and endpoints for the streaklines from the image of κ and then used geodesic curves to connect them. We defined a cost function ψ in the form:

$$\psi = \begin{cases} 1 - e^{-k_1\kappa} + e^{-k_2c}, & \text{for high concentration streaks.} \\ 1 - e^{k_1\kappa} + e^{k_2(c-\max(c))}, & \text{for low concentration streaks.} \end{cases} \quad (1)$$

where k_1 and k_2 are parameters controlling how strongly the geodesics follow the curvature and the concentration fields, respectively, and were determined by trial-and-error. A low value of k_1 or k_2 will connect the start and end points with a straight line, irrespective of the underlying curvature or concentration fields. Higher values will cause the geodesics to follow features in the fields more closely, but a value that is too high can cause erratic jumps because the geodesics become too sensitive to small differences in κ or c (Figure S1 in Supporting Information S1). Once ψ was defined, we computed the geodesic distance of each pixel from the start point, and extracted the geodesic by following the steepest descent path from the end point to the start point (Figure 2c). We sometimes needed to select multiple points along the same streakline to prevent geodesics from “jumping” to neighboring streaklines, and additionally prevented streaklines from crossing each other by setting previously extracted streaks to infinite cost.

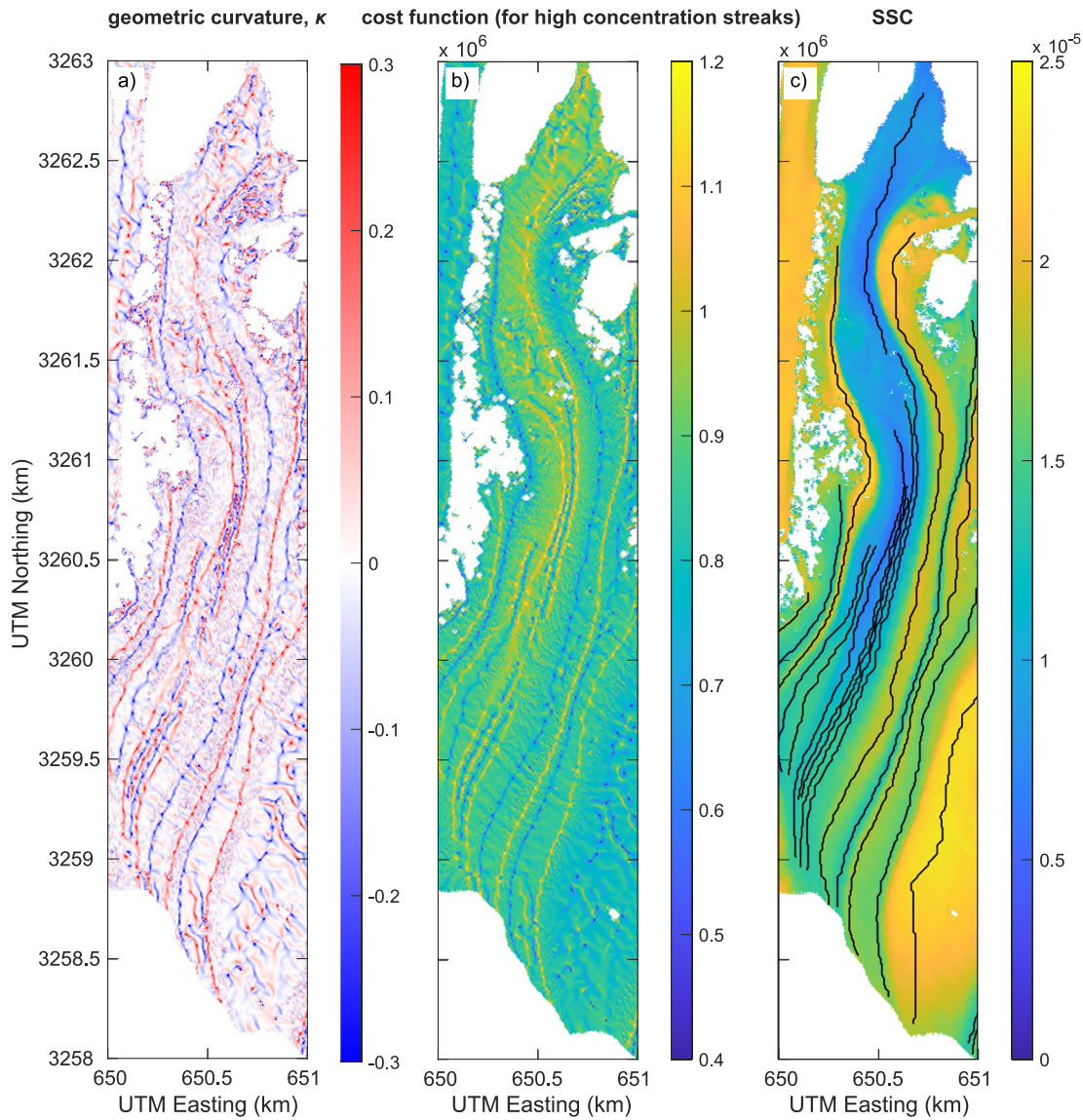


Figure 2. Procedure for extracting streaklines from image of suspended sediment concentration (SSC). (a) Geometric curvature κ of remote-sensed SSC. (b) Cost function derived from geometric curvature and SSC. Low concentration (positive κ) streaks have high cost, and high concentration streaks have low cost. (c) Extracted streaklines overlaying the map of SSC.

2.2. Inferring Deposition/Erosion Rates

Next, we developed a method for using sediment concentration along streaklines to invert for deposition/erosion rates. The depth-averaged mass balance for sediment in the water column can be written:

$$\frac{\partial (h\bar{c})}{\partial t} + \frac{\partial (uh\bar{c})}{\partial x} + \frac{\partial (vh\bar{c})}{\partial y} = w_s(E - c_b) + \epsilon \left(\frac{\partial}{\partial x} \left(h \frac{\partial \bar{c}}{\partial x} \right) + \frac{\partial}{\partial y} \left(h \frac{\partial \bar{c}}{\partial y} \right) \right) \quad (2)$$

where h is the flow depth, \bar{c} is the depth-averaged sediment concentration, u and v are the x and y components of the depth-averaged flow velocity, w_s is the settling velocity, E is bed-sediment entrainment rate, c_b is the near-bed concentration, and ϵ is the sediment diffusivity (Spasojevic & Holly, 1990). We simplified Equation 2 by combining it with the equation for water mass conservation, using a streakline-oriented coordinate system, and making the assumptions of steady state and negligible diffusivity, which we discuss later (see Text S1 in Supporting Information S1). Additionally, we assumed that the depth-averaged concentration \bar{c} can be approximated as

the near-surface remote-sensed SSC c , which is reasonable because over 90% of the sediment transported in Wax Lake Delta is mud (Olliver et al., 2020). The resulting expression is:

$$-h\|\vec{v}\|\frac{\partial c}{\partial s} = D \quad (3)$$

where $\|\vec{v}\|$ is the magnitude of the depth-averaged flow velocity, s is the down-streakline distance, and D is the net-deposition rate, given by $D = w_s(c_b - E)$, which is positive for deposition and negative for erosion, and is equivalent to the rate of elevation change not accounting for porosity or subsidence. Notably, even though an estimate of flow depth and velocity magnitude are needed to obtain D , the sign of D depends only on $\frac{\partial c}{\partial s}$, meaning that areas of erosion and deposition can be identified without any additional information. However, in order to make a quantitative estimate of D , we needed to obtain an estimate of h and $\|\vec{v}\|$. We obtained these values using a previously-developed calibrated hydrodynamic model of Wax Lake Delta. This model uses ANUGA software to solve the depth-averaged shallow water equations on an unstructured grid (Wright et al., 2022; Zerger & Argent, 2005). The model was calibrated against water level time series from 40 gages as well as maps of InSAR-derived water level change, as described by Wright et al. (2022). We simulated a time period that included the AVIRIS-NG flyover, providing values for h and $\|\vec{v}\|$. With these values, we applied Equation 3 to the extracted streaks to obtain values of net-deposition D along all extracted streaklines. To remove small-scale noise associated with taking the derivative of c , we applied a down-streak low-pass filter of 200 pixels and additionally a moving average of 100 pixels, with a pixel size of 5.4 m.

In order to test the validity of our method, we developed a simple add-on sediment advection and settling model, which we ran using hydrodynamic output from the ANUGA model (Text S2 in Supporting Information S1). The sediment model solves Equation 2 under the assumptions of zero entrainment and diffusivity, and with a uniform vertical SSC profile, that is, $c_b = \bar{c}$. We used a settling velocity of 0.1 mm/s, and used an explicit finite volume algorithm with a van Leer flux limiter to solve for sediment advection. Our purpose with this simple model was not to accurately model SSC, which is highly complex, but rather to explore whether our methodology yields accurate results in a simple synthetic case where the deposition rate is known, before applying the method to the real remote-sensed SSC.

3. Results

First, to validate our method, we used our 2D sediment model from which we compared our streakline-based inference of the net-deposition rate D to the actual simulated deposition rates from the settling flux cw_s . Based on the sediment model, Figure 3 shows a comparison between the actual simulated D and D inferred using the streakline method across Wax Lake Delta for the time period corresponding to the AVIRIS-NG flyover. We found that the streakline-derived patterns of D are nearly identical to the true simulated sedimentation, even though the streakline method does not require independent measurement of the flow direction or the settling velocity. This shows that the steady-state assumption used in deriving Equation 3 does not strongly affect the results. There was one instance of erroneous negative inferred D based on the streakline method, highlighted in the insets of Figures 3b and 3c, which occurred where a low-concentration streakline originating from an island interior reentered a high concentration channel. Here, high and low concentration streaklines were forced to converge into a narrow channel, and the low concentration streakline had a downstream increase in concentration associated with numerical diffusion from neighboring streaklines.

With our method validated, we applied it to the true remote-sensed SSC. Patterns of net-erosion versus net-deposition can be inferred from the sign of $\frac{\partial c}{\partial s}$ alone, with $\frac{\partial c}{\partial s} > 0$ implying erosion, and $\frac{\partial c}{\partial s} < 0$ implying deposition. To make a quantitative estimate of D , we additionally used depth h and velocity magnitude $\|\vec{v}\|$ from the ANUGA hydrodynamic model along with $\frac{\partial c}{\partial s}$ from the streaklines to generate the pattern of instantaneous net-deposition rates shown in Figure 4. We found areas of net-deposition and net-erosion, with typical values of D ranging from -10 to 10 cm/yr (11.4 $\mu\text{m/hr}$), not accounting for porosity, and some areas with very little change. We found coherent spatial patterns in the map of D . In particular, areas of net-erosion are concentrated on the eastern delta front, as well as some of the downstream portions of island interiors (e.g., Figure 4d). Areas of net-deposition are concentrated on channel-bordering island margins (e.g., Figure 4c) and the downstream portions of some sediment plumes. We also identified a few areas where sediment diffusion is likely affecting results. Diffusion should

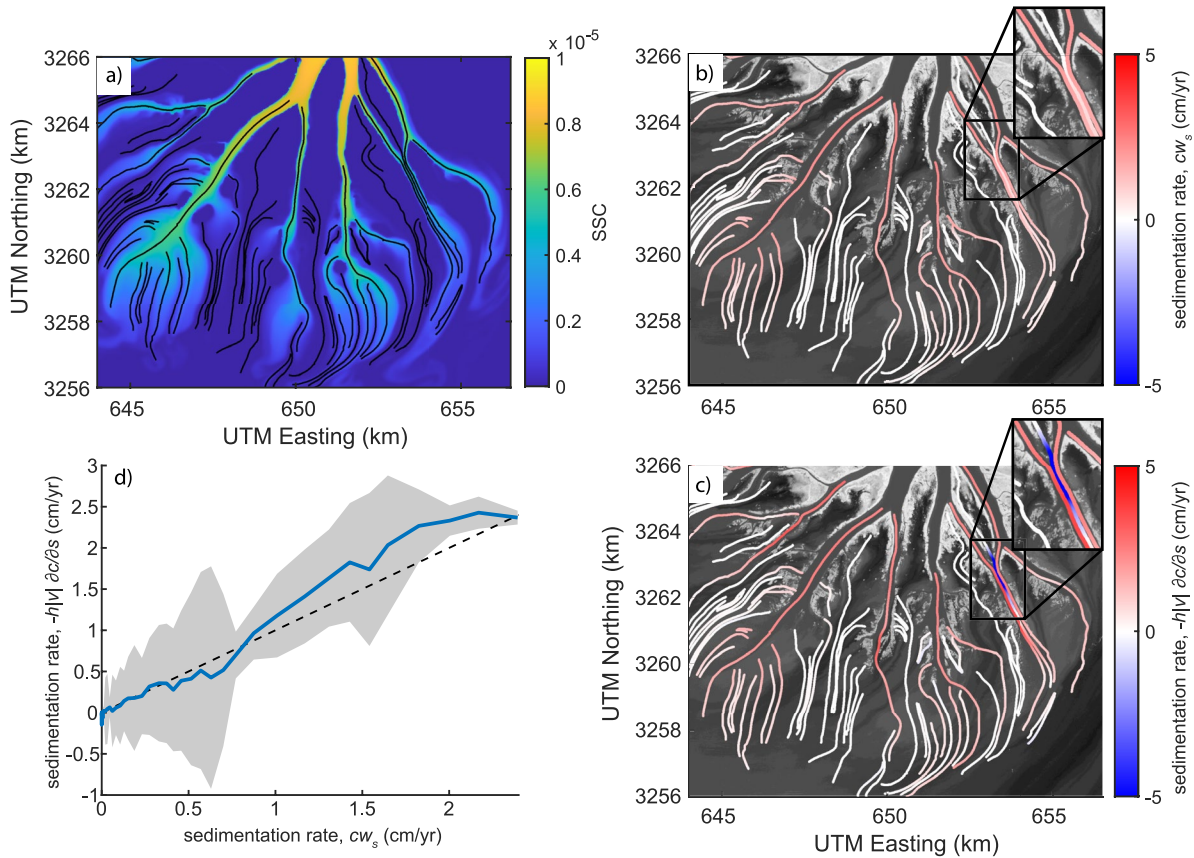


Figure 3. (a) Simulated suspended sediment concentration (SSC) from 2D sediment advection-settling model using hydrodynamic output from ANUGA, overlaid by extracted streaklines. Simulation corresponds to 15:33 GMT on 18 October 2016. (b) True modeled sedimentation rate, calculated as cw_s . (c) Inferred sedimentation rate from streakline method, $-|h|\vec{v} \cdot \frac{\partial c}{\partial s}$. Inset shows a region of poor agreement between inferred and simulated sedimentation rates due to diffusion between streaklines. (d) Comparison between inferred sedimentation from streakline method and simulated sedimentation rate, with blue line indicating the mean and gray shading indicating standard deviation, using a bin size of 500 points (22,563 total points). Dashed line indicates 1:1 correspondence.

produce an alternating pattern of D for neighboring streaklines, as positive-curvature (low concentration) streaks gain sediment at the expense of their negative-curvature (high concentration) neighboring streaks. We found an alternating pattern in a portion of the image that appears to be affected by a shear instability (Figure 4b) and part of one of the islands where there is strong convergence of streaklines (Figure 4c). However, the coherent patterns shared by neighboring streaks of positive and negative curvature suggest that diffusion is of second-order importance in most areas. The mean net-deposition rate D averaging over all streaklines was -0.27 cm/yr ($-0.31 \mu\text{m/hr}$), that is, net erosion. Averaging over only portions of streaks with positive net-deposition yields a mean deposition rate of 1.19 cm/yr ($1.36 \mu\text{m/hr}$), and averaging over areas of net-erosion yields a mean erosion rate of -1.56 cm/yr ($1.78 \mu\text{m/hr}$). These values should not be interpreted as delta-wide averages because we have not attempted to account for spacing between streaklines, and even though we report values in units of cm/yr, they are instantaneous rates.

4. Discussion

This study shows for the first time how synoptic patterns of instantaneous erosion and deposition along streaklines can be inferred from remote-sensed sediment concentration alone. This allows for the possibility of directly relating deposition/erosion patterns to specific hydrodynamic and environmental conditions at the same timescale. Previous studies have been limited by the long time interval between measurements of bathymetric change, making it difficult to mechanistically link flow conditions to deposition and erosion. For instance, Shaw et al. (2016) found that areas of positive convective flow acceleration tended to coincide with erosion, and

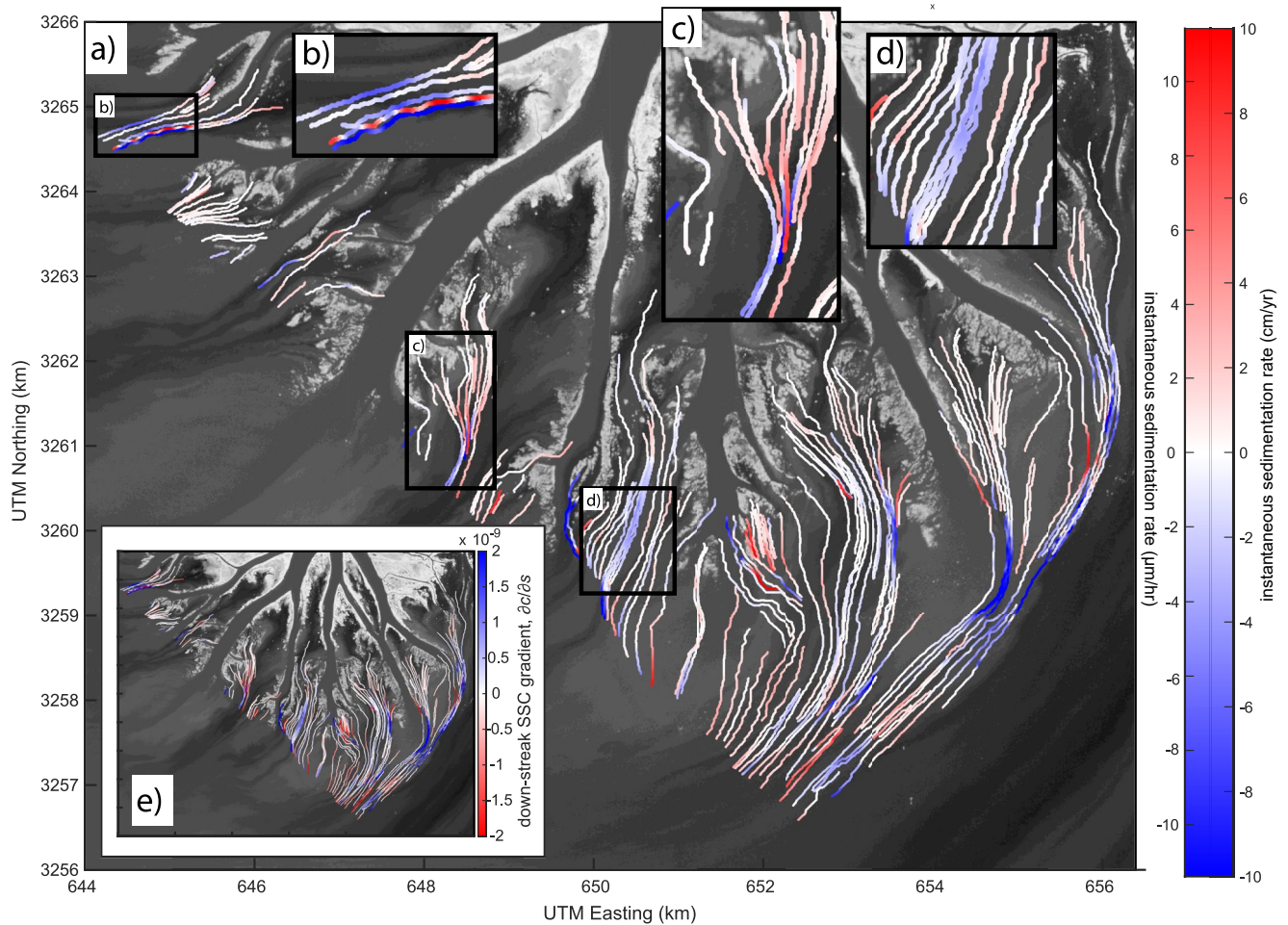


Figure 4. (a) Map of inferred instantaneous sedimentation rate from the streakline method, based on remote-sensed suspended sediment concentration (SSC) from 18 October 2016, and depth and velocity magnitude values from the ANUGA hydrodynamic model. Positive sedimentation rate (red) indicates net-deposition, and negative sedimentation rate (blue) indicates net-erosion. Insets (b–d) highlight details from the sedimentation rate map. (e) Map of down-streak SSC gradient, $\frac{\partial c}{\partial s}$, based on remote-sensed SSC from 18 October 2016. Positive values (blue) indicate net-erosion, and negative values (red) indicate net-deposition.

areas of negative convective flow acceleration coincided with deposition. However, they found discrepancies due to comparing flow conditions at a single instant in time to bathymetric change over 13 months. Our new streakline-based method for inferring instantaneous patterns of bathymetric change could provide a better test of hypotheses such as the link between convective flow acceleration and deposition/erosion proposed by Shaw et al. (2016). In order to generate a quantitative estimate of erosion/deposition rates, we needed values for flow velocity magnitude and flow depth, which we acquired from a hydrodynamic model. However, as can be seen by comparing Figures 4a and 4e, the qualitative patterns inferred from $\frac{\partial c}{\partial s}$ alone agree well with the patterns generated when flow depth and velocity are included; for many applications the sign of bathymetric change is useful even if the rates are not known. There is also the possibility of generating the flow velocity map from remote sensing (Ayoub et al., 2018), which combined with the streakline method applied to SSC, could provide a means to estimate instantaneous sedimentation rates from remote sensing alone.

Our detected deposition/erosion patterns shown in Figure 4 represent a single snapshot of longer-term patterns of deposition and erosion. We find instantaneous rates ranging from net-deposition to net-erosion on the order of ± 10 cm/yr. However, if we average spatially across all streaklines, we obtain a net-deposition rate of -0.27 cm/yr, that is, the average rate is significantly smaller in magnitude than the rates observed in particular areas. Excluding regions of net-erosion, we obtain an average net-deposition rate of 1.19 cm/yr, which is on the order of relative sea level rise rates in the region (Jankowski et al., 2017). We do not have any temporal data available, but it is

possible that spatial patterns of erosion and deposition at a different snapshot in time could partially compensate for the patterns we observe here, yielding a long-term pattern that is more uniform. Intriguingly, the longer-term pattern of erosion/deposition measured between bathymetric surveys in February 2015 and July 2016 by Whaling and Shaw (2020) was largely the opposite of what we observed; they found widespread erosion, with particularly high rates near the levees, and the eastern delta front was one of the few areas where they observed net-deposition. However, like Whaling and Shaw (2020), we found erosion in some island interiors, as shown in Figure 4d. Whaling and Shaw (2020) attributed the widespread erosion they observed to the effect of resuspension due to winter storms. Our results indicate that erosion is not limited to events such as cold fronts, and can occur with low river flows and typical tides. The patterns we observed under non-storm conditions could be partially compensating for bathymetric changes during winter storms.

The streakline inversion provides insight into how flow conditions, sediment transport, and bathymetric change are interlinked in Wax Lake Delta. The 18 October 2016 AVIRIS-NG flight occurred under low river flow conditions (USGS Calumet gage discharge of $1,600 \text{ m}^3 \text{ s}^{-1}$) towards the tail end of a long period of falling tide (Figure S2 in Supporting Information S1). We compared a map of flow velocity magnitude generated by the ANUGA hydrodynamic model (Figure S3 in Supporting Information S1) to the deposition/erosion patterns shown in Figure 4. We found that areas of net-deposition were particularly prevalent along channel-bordering island margins. These were areas where the ANUGA model indicates that flow velocities were low, suggesting limited sediment entrainment, and where there was high sediment supply from the surrounding channels. In contrast, downstream central portions of island interiors tended to be net-erosional. This is consistent with the relatively high flow velocities observed in the ANUGA model, which drives entrainment of sediment from the bed, as well as reduced sediment supply from upstream due to sequestration on the island levees, limiting the potential for sedimentation. The highest net-erosion rates we observed occurred along the eastern delta front. This is a region where the ANUGA model indicates that influence from the Atchafalaya Delta to the east generates higher flow velocities. Our finding of strong net-erosion associated with this region may explain why the delta foreset is significantly steeper in the eastern portion of the delta than elsewhere (Shaw et al., 2016). Other portions of the delta-front are net-depositional, associated with lower flow velocities in conjunction with high sediment supply. Overall, our results showed that high sediment concentrations and low flow velocities were associated with net-deposition, whereas high flow velocities were associated with net-erosion.

Our methods could be applied at other snapshots in time or in other deltas to explore more broadly the relationship between instantaneous flow conditions and patterns of deposition and erosion. However, there are some limitations to applying our method. The first is that streaklines must be visible in remote-sensed SSC. This requires that the streaklines are present, that the image resolution is sufficient to capture them, and that the accuracy of the measurements is high enough for streaklines to be differentiated and for measurements of $\frac{\partial c}{\partial s}$. We note that streaklines are not always present, and that the presence/absence of streaklines may be related to hydrodynamic conditions. We found that the AVIRIS-NG acquisition from 17 October 2016, did not have visible streaklines, unlike the acquisition the following day (Figure S4 in Supporting Information S1). Tidal cycle may play a role; the October 17 flight was during a period of rising tide, whereas the October 18 flight with visible streaklines took place near the end of a long period of falling tide (Figure S2 in Supporting Information S1). This is consistent with Cathcart et al. (2020), who found that under low river discharge, rising tide inhibited streaklines. Additionally, for the October 17 flight, diffuse regions of high SSC in island interiors could be a consequence of wave-driven sediment resuspension. Another potential limitation is diffusion of sediment, but we found by comparing rates along neighboring streaks with opposite signs of curvature that except in a few areas with strong flow convergence and/or shear instabilities, diffusion was of second-order importance, consistent with the findings from Shaw et al. (2016) and Ayoub et al. (2018) that turbulent mixing of flow streaks is rare in Wax Lake Delta. Finally, in deriving Equation 3, we assumed that the streakline orientation was the same as the depth-averaged flow direction. This assumption may be violated under highly unsteady flow conditions produced by tides. Ayoub et al. (2018) and Cathcart et al. (2020) found that the assumption that streaklines are oriented with the flow direction tends to hold in Wax Lake Delta, although low flow conditions with rising tide were more likely to yield discrepancies between the streakline and flow orientations.

We emphasize that our method provides an estimate of instantaneous deposition/erosion based on patterns in the near-surface SSC under the assumption of a uniform vertical SSC profile. Although this assumption is typically appropriate for mud, which makes up the majority of the sediment transport in Wax Lake Delta and is well-mixed

vertically due to its low Rouse number (Rouse, 1937), sand concentrations are typically much higher near the bed than near the water surface. Therefore, there may be decorrelation between the patterns we observe for mud and the evolution of sandy deposits, such as levees (Wellner et al., 2005), and our method would produce significant errors in deltas dominated by sediment coarser than mud. However, our method may still provide a useful estimate of mud erosion and deposition within these regions, even if the bathymetric change is dominated by sand. Additionally, whereas Wax Lake Delta enters the shallow freshwater Atchafalaya Bay (Shaw et al., 2013), in other deltas, particularly in marine environments, processes such as plume settling, density stratification, subaqueous sediment density flows, and estuarine circulation can yield near-bed patterns of sediment transport that are drastically different from near-surface patterns (Geyer et al., 2004; Hizzett et al., 2018; Officer, 1976). To our knowledge, these processes have not been observed in Wax Lake Delta. Despite these important caveats, our method provides a useful way to estimate instantaneous bathymetric change due to settling and entrainment under conditions where the vertical SSC profile is relatively uniform.

Future work could apply the methods developed here to different flow conditions and/or different locations, including wetlands and other river deltas. The NASA Delta-X mission will provide new AVIRIS-NG data for the western Mississippi Delta, including Wax Lake Delta. The Delta-X mission will provide a near ideal remote sensing and field data set to observe these streaks at different tidal conditions and discharges, and with fine spatial resolution of AVIRIS-NG. The observed streaks, while extending multiple kilometers, are only tens to a few hundreds of meters wide, and therefore require fine spatial resolution to extract. Additionally, inferring sedimentation rates from streaklines requires sufficient spectral resolution to resolve SSC changes along streaks. For example, to measure a sedimentation rate of 1 cm/yr over a distance of 1 km, and assuming a depth of 1 m and velocity of 0.2 m/s typical of this study, SSC differences on the order of 10^{-6} must be resolved. The Surface Biology and Geology (SBG) mission is designed to address the Decadal Survey 's objectives to track aquatic biogeochemistry (NASEM 2018) and will provide the required data quality to replicate our results globally. The SBG mission (Cawse-Nicholson et al., 2021) will provide hyperspectral observations globally, including at coastal interfaces, every few weeks with spatial resolutions ranging between 30 and 45 m. Its spectral resolution and range enable accurate estimates of sediment concentrations, and its spatial resolution can resolve streaks. The fast repeat provides a dense time-series data set that increases the probability to image cloud-free landscapes and various hydrological conditions. Otherwise, the current spaceborne constellation of sensors from Landsat, Sentinel-2, Sentinel-3 (Pahlevan et al., 2022) and Planet can resolve streaks but contribute limited information about sediment concentrations. Hyperspectral (or imaging spectroscopy) data are necessary to attain site-agnostic and high accuracy estimates of sediment concentrations (e.g., Jensen et al. (2019)) to support applications of our model globally.

5. Conclusions

1. We developed a new method for inferring instantaneous synoptic patterns of deposition and erosion in river deltas from a map of remotely-sensed suspended sediment concentration, providing for the first time a way to mechanistically link hydrodynamic and environmental conditions to instantaneous rates of bathymetric change.
2. Following a semi-automated approach, we extracted streaklines using a cost function based on the concentration and geometric curvature of the concentration as curves of minimum geodesic distance.
3. We tested our method for inferring patterns of deposition and erosion from the change in sediment concentration along streaklines using synthetic data from a 2D sediment advection and settling model, and found that our method accurately inverts for deposition rates.
4. We obtained coherent patterns of deposition and erosion, with deposition focused on the channel-bounded margins of islands, and erosion focused in island interiors and the eastern delta front, and link these patterns to prevailing hydrodynamic conditions.
5. Our results could be applied to different time periods or different river deltas to better understand their bathymetric evolution, highlighting the need for high-resolution maps of remote-sensed suspended sediment concentration in river deltas worldwide.

Data Availability Statement

Code for the sediment advection/settling model can be downloaded from https://github.com/salterg/sediment_advection_settling. Suspended sediment concentration data can be downloaded from the Oak Ridge National Laboratory Distributed Active Archive Center (Jensen et al., 2021).

Acknowledgments

The NASA Delta-X project is funded by the Science Mission Directorate's Earth Science Division through the Earth Venture Suborbital-3 Program NNH17ZDA001N-EVS3. This work was partly conducted by the Jet Propulsion Laboratory, California Institute of Technology, under contract with the National Aeronautics and Space Administration. We thank John Shaw, Chris Cathcart, and an anonymous reviewer for insightful feedback on our manuscript. We also thank Sergio Fagherazzi and members of the Delta-X team for insightful discussions. Suspended sediment concentration data acquisition was supported by Jet Propulsion Laboratory Research and Technology Development (JPL-R&TD) FY17–19 (grant 01STCR/R.17.231.069).

References

- Ayoub, F., Jones, C., Lamb, M., Holt, B., Shaw, J., Mohrig, D., & Wagner, W. (2018). Inferring surface currents within submerged, vegetated deltaic islands and wetlands from multi-pass airborne SAR. *Remote Sensing of Environment*, 212, 148–160. <https://doi.org/10.1016/j.rse.2018.04.035>
- Bevington, A. E., Twilley, R. R., Sasser, C. E., & Holm, G. O. (2017). Contribution of river floods, hurricanes, and cold fronts to elevation change in a deltaic floodplain, northern Gulf of Mexico, USA. *Estuarine, Coastal and Shelf Science*, 191, 188–200. <https://doi.org/10.1016/j.ecss.2017.04.010>
- Carle, M. V., Sasser, C. E., & Roberts, H. H. (2015). Accretion and vegetation community change in the Wax Lake Delta following the historic 2011 Mississippi River flood. *Journal of Coastal Research*, 31(3), 569–587. <https://doi.org/10.2112/jcoastres-d-13-00109.1>
- Cathcart, C., Shaw, J. B., & Amos, M. (2020). Validation of streaklines as recorders of synoptic flow direction in a deltaic setting. *Remote Sensing*, 12(1), 148. <https://doi.org/10.3390/rs12010148>
- Cause-Nicholson, K., Townsend, P. A., Schimel, D., Assiri, A. M., Blake, P. L., Buongiorno, M. F., et al. (2021). NASA's surface biology and geology designated observatory: A perspective on surface imaging algorithms. *Remote Sensing of Environment*, 257, 112349. <https://doi.org/10.1016/j.rse.2021.112349>
- Chapman, J. W., Thompson, D. R., Helmlinger, M. C., Bue, B. D., Green, R. O., Eastwood, M. L., et al. (2019). Spectral and radiometric calibration of the next generation airborne visible infrared spectrometer (AVIRIS-NG). *Remote Sensing*, 11(18), 2129. <https://doi.org/10.3390/rs11182129>
- Curran, P. J., & Novo, E. M. M. (1988). The relationship between suspended sediment concentration and remotely sensed spectral radiance: A review. *Journal of Coastal Research*, 4(3), 351–368. Retrieved from <http://www.jstor.org/stable/4297423>
- Fichot, C. G., Downing, B. D., Bergamaschi, B. A., Windham-Myers, L., Marvin-Dipasquale, M., Thompson, D. R., & Gierach, M. M. (2016). High-resolution remote sensing of water quality in the San Francisco Bay-Delta Estuary. *Environmental Science and Technology*, 50(2), 573–583. <https://doi.org/10.1021/acs.est.5b03518>
- Geyer, W., Hill, P., & Kineke, G. (2004). The transport, transformation and dispersal of sediment by buoyant coastal flows. *Continental Shelf Research*, 24(7), 927–949. <https://doi.org/10.1016/j.csr.2004.02.006>
- Hizzett, J. L., Hughes Clarke, J. E., Sumner, E. J., Cartigny, M. J. B., Talling, P. J., & Clare, M. A. (2018). Which triggers produce the most erosive, frequent, and longest runout turbidity currents on deltas? *Geophysical Research Letters*, 45(2), 855–863. <https://doi.org/10.1002/2017GL075751>
- Jankowski, K. L., Törnqvist, T. E., & Fernandes, A. M. (2017). Vulnerability of Louisiana's coastal wetlands to present-day rates of relative sea-level rise. *Nature Communications*, 8(1), 14792. <https://doi.org/10.1038/ncomms14792>
- Jensen, D., Simard, M., Cavanaugh, K., Sheng, Y., Fichot, C. G., Pavelsky, T., & Twilley, R. (2019). Improving the transferability of suspended solid estimation in wetland and deltaic waters with an empirical hyperspectral approach. *Remote Sensing*, 11(13), 1629. <https://doi.org/10.3390/RS11131629>
- Jensen, D., Simard, M., Fichot, C., & Pavelsky, T. (2021). *Pre-delta-X: AVIRIS-derived Total Suspended Solids Maps for MRD, LA, USA, 2015–2016*. ORNL Distributed Active Archive Center. Retrieved from https://daac.ornl.gov/cgi-bin/dsvviewer.pl?ds_id=1822
- Officer, C. B. (1976). *Physical oceanography of estuaries (and associated coastal waters)*. Wiley-Interscience.
- Olliver, E. A., Edmonds, D. A., & Shaw, J. B. (2020). Influence of floods, tides, and vegetation on sediment retention in Wax Lake Delta, Louisiana, USA. *Journal of Geophysical Research: Earth Surface*, 125(1). <https://doi.org/10.1029/2019JF005316>
- Olmanson, L. G., Brezonik, P. L., & Bauer, M. E. (2013). Airborne hyperspectral remote sensing to assess spatial distribution of water quality characteristics in large rivers: The Mississippi River and its tributaries in Minnesota. *Remote Sensing of Environment*, 130, 254–265. <https://doi.org/10.1016/j.rse.2012.11.023>
- Pahlevan, N., Smith, B., Alikas, K., Anstee, J., Barbosa, C., Binding, C., et al. (2022). Simultaneous retrieval of selected optical water quality indicators from Landsat-8, Sentinel-2, and Sentinel-3. *Remote Sensing of Environment*, 270, 112860. <https://doi.org/10.1016/j.rse.2021.112860>
- Passalacqua, P., Trung, T. D., Fofoula-Georgiou, E., Sapiro, G., & Dietrich, W. E. (2010). A geometric framework for channel network extraction from lidar: Nonlinear diffusion and geodesic paths. *Journal of Geophysical Research*, 115(F1), F01002. <https://doi.org/10.1029/2009JF001254>
- Peckham, S. D. (2008). A new method for estimating suspended sediment concentrations and deposition rates from satellite imagery based on the physics of plumes. *Computers & Geosciences*, 34(10), 1198–1222. <https://doi.org/10.1016/j.cageo.2008.02.009>
- Perona, P., & Malik, J. (1990). Scale-space and edge detection using anisotropic diffusion. *IEEE Transactions on Pattern Analysis and Machine Intelligence*, 12(7), 629–639. <https://doi.org/10.1109/34.56205>
- Rouse, H. (1937). Modern conceptions of the mechanics of fluid turbulence. *Transactions of the American Society of Civil Engineers*, 102(1), 463–505. <https://doi.org/10.1061/taceat.0004872>
- Shaw, J. B., & Mohrig, D. (2014). The importance of erosion in distributary channel network growth, Wax Lake Delta, Louisiana, USA. *Geology*, 42(1), 31–34. <https://doi.org/10.1130/G34751.1>
- Shaw, J. B., Mohrig, D., & Wagner, R. W. (2016). Flow patterns and morphology of a prograding river delta. *Journal of Geophysical Research: Earth Surface*, 121(2), 372–391. <https://doi.org/10.1002/2015JF003570>
- Shaw, J. B., Mohrig, D., & Whitman, S. K. (2013). The morphology and evolution of channels on the Wax Lake Delta, Louisiana, USA. *Journal of Geophysical Research: Earth Surface*, 118(3), 1562–1584. <https://doi.org/10.1002/jgrf.20123>
- Simard, M., Denbina, M. W., Wright, K. A., & Jensen, D. (2020). The Delta-X Framework: A Reality Check for Hydrodynamic, Sediment Transport and Ecogeomorphic Models. In *Ocean sciences meeting*.
- Spasojevic, M., & Holly, F. M., Jr. (1990). 2-d bed evolution in natural watercourses—New simulation approach. *Journal of Waterway, Port, Coastal, and Ocean Engineering*, 116(4), 425–443. [https://doi.org/10.1061/\(ASCE\)0733-950X](https://doi.org/10.1061/(ASCE)0733-950X)
- Styles, R., Snedden, G. A., Smith, S. J., Bryant, D. B., Boyd, B. M., Gailani, J. Z., et al. (2021). Seasonal Controls on Sediment Delivery and Hydrodynamics in a Vegetated Tidally Influenced Interdistributary Island. *Journal of Geophysical Research: Oceans*, 126(7), e2020JC016146. <https://doi.org/10.1029/2020JC016146>

- Thompson, D. R., Gao, B.-C., Green, R. O., Roberts, D. A., Dennison, P. E., & Lundeen, S. R. (2015). Atmospheric correction for global mapping spectroscopy: ATREM advances for the HypsIRI preparatory campaign. *Remote Sensing of Environment*, *167*, 64–77. <https://doi.org/10.1016/j.rse.2015.02.010>
- Van der Wal, D., Van Kessel, T., Eleveld, M. A., & Vanlede, J. (2010). Spatial heterogeneity in estuarine mud dynamics. *Ocean Dynamics*, *60*(3), 519–533. <https://doi.org/10.1007/s10236-010-0271-9>
- Wagner, W., Lague, D., Mohrig, D., Passalacqua, P., Shaw, J., & Moffett, K. (2017). Elevation change and stability on a prograding delta. *Geophysical Research Letters*, *44*, 1786–1794. <https://doi.org/10.1002/2016GL072070>
- Wellner, R., Beaubouef, R., Van Wagoner, J., Roberts, H., & Sun, T. (2005). *Jet-plume depositional bodies—the primary building blocks of wax lake delta*.
- Whaling, A., & Shaw, J. (2020). Changes to subaqueous delta bathymetry following a high river flow event, Wax Lake Delta, USA. *Estuaries and Coasts*, *43*(8), 1923–1938. <https://doi.org/10.1007/s12237-020-00727-y>
- Wright, K., Passalacqua, P., Simard, M., & Jones, C. E. (2022). Integrating connectivity into hydrodynamic models: An automated open-source method to refine an unstructured mesh using remote sensing. *EarthArXiv*. <https://doi.org/10.31223/X57K9V>
- Zerger, A., & Argent, R. (2005). *Hydrodynamic modelling of coastal inundation*. Modelling and Simulation Society of Australia and New Zealand.